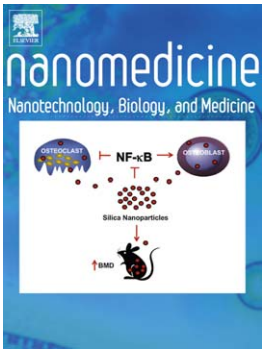

Multiscale benchmarking of drug delivery vectors

Huw D. Summers, Matthew J. Ware, Ravish Majithia, Kenith E. Meissner, Biana Godin, Paul Rees

PII: S1549-9634(16)30024-7
DOI: doi: 10.1016/j.nano.2016.03.006
Reference: NANO 1317

To appear in: *Nanomedicine: Nanotechnology, Biology, and Medicine*

Received date: 7 September 2015
Revised date: 8 January 2016
Accepted date: 28 March 2016

Please cite this article as: Summers Huw D., Ware Matthew J., Majithia Ravish, Meissner Kenith E., Godin Biana, Rees Paul, Multiscale benchmarking of drug delivery vectors, *Nanomedicine: Nanotechnology, Biology, and Medicine* (2016), doi: 10.1016/j.nano.2016.03.006

Multiscale benchmarking of drug delivery vectors

Huw D. Summers, Matthew J. Ware, Ravish Majithia, Kenith E. Meissner, Biana Godin and Paul Rees

Huw D. Summers*, Paul Rees,

College of Engineering, Swansea University, SA2 8PP, U.K.

E-mail: h.d.summers@swansea.ac.uk; p.rees@swansea.ac.uk;

* Corresponding author, tel. +44 1792 602915

Matthew J. Ware[1], Biana Godin,

Department of Nanomedicine, Houston Methodist Research Institute, Houston, Texas 77030, USA

[1] current address: Baylor College of Medicine, Department of Surgery, One Baylor Plaza,R 550 Houston, TX 77030

Matthew.Ware@bcm.edu; bgodin@houstonmethodist.org

R. Majithia, Kenith E. Meissner[2]

Department of Biomedical Engineering, Texas A&M University, College Station, Texas, USA

[2] current address: College of Engineering, Swansea University, SA2 8PP, U.K.

k.meissner@swansea.ac.uk;

Huw D. Summers and Biana Godin are joint senior authors.

Abstract word count = 150, Manuscript word count = 5475

Number of figures/tables = 8, number of references = 48

Keywords: dose-response assays, nanoparticles, drug delivery, nanomedicine, nanotoxicology

Acknowledgements

MJ Ware acknowledges the Swansea University and Houston Methodist Research Institute Joint Ph.D. Graduate Program and the funding received from the Engineering and Physical Sciences Research Council, U.K. We also acknowledge the support of the HMRI Advanced Cellular and Tissue Microscope Core Facility where time lapse imaging was performed. BG and MW

acknowledge the financial support from NIH U54CA143837 Physical Sciences and Oncology grant. BG acknowledges the financial support from NIH 1U54CA151668-01 Cancer Centre for Nanotechnology Excellence grant.

ABSTRACT

Cross-system comparisons of drug delivery vectors are essential to ensure optimal design. An in-vitro experimental protocol is presented that separates the role of the delivery vector from that of its cargo in determining the cell response, thus allowing quantitative comparison of different systems. The technique is validated through benchmarking of the dose-response of human fibroblast cells exposed to the cationic molecule, polyethylene imine (PEI); delivered as a free molecule and as a cargo on the surface of CdSe nanoparticles and Silica microparticles. The exposure metrics are converted to a delivered dose with the transport properties of the different scale systems characterized by a delivery time, τ. The benchmarking highlights an agglomeration of the free PEI molecules into micron sized clusters and identifies the metric determining cell death as the total number of PEI molecules presented to cells, determined by the delivery vector dose and the surface density of the cargo.

1. Background

A drug molecule or imaging payload must reach its intended site of action to exert an efficient therapeutic or diagnostic action and to prevent adverse side effects.[1,2] The delivery of active agents to the target organ or disease loci generally requires negotiation of numerous bio-barriers mainly comprised of cells from different origins.[3–5] Consequently, there has been a rapid development in novel nano and micro-scale vectors to more efficiently deliver drugs, genetic material, and imaging contrast agents to their target locations.[6–8] While particulates can be administered locally or systemically through various routes (e.g. dermal, intravenous, oral, pulmonary), their initial performance evaluation includes *in vitro* studies in cell cultures.

In this work, we use the "on contact" toxicity of PEI as a probe of the dynamics of arrival to the cell surface of the same material in carriers of different sizes. In general, this assessment is very important as the dynamic of arrival can further be translated to multiple biological outputs (toxicity being one of them). It is becoming increasingly evident that nano and micro materials cannot be treated in the same manner as chemical compounds with regards to their safety and efficacy assessment [9], as their unique physicochemical properties are responsible for unexpected interactions with experimental and biological systems [10,11]. Despite the wide use of in vitro systems for biological assessment of NPs, the direct measure of cellular dosimetry has largely been overlooked in favour of using overall metrics of exposure, principally particle concentration on a mass [12], number, or surface area basis. This is due to the difficulties in measuring particle arrival at the cell interface. In this context, below we discuss various tests for evaluation of biological (toxicity/efficacy) responses as well the effects of particles of different sizes on the above.

In general, there is an urgent need in toxicity tests or dose response assays to de-couple the physical effects acting upon a particle from their biological effects so that true biological response to

variables such as particle size or shape can be determined. This is particularly important in investigations which are directly comparing cellular responses across multiple materials or materials of different sizes [13–15]. However, physical effects in a system are commonly ignored and the cellular response observed is thought to be solely biology-driven, which may generally lead to misinterpretation of the obtained results. For instance, cytotoxicity assays investigating the role of cell cycle in cellular uptake and toxicity do not take into account the non-linear delivery rate of nano and micro-particles and consider responses to be uniquely driven by biological changes in the cell during proliferation [16]. In terms of the efficacy, the rate of arrival of an agent to the cell surface is extremely important when comparing therapeutic entities such as low molecular weight drugs, proteins and oligonucleotides adsorbed/conjugated to the surface of the carriers [17,18]. In this instance, decoupling the kinetic processes of carrier arrival to the cell surface and the ultimate response will allow for better understanding of the mechanism of action of various carriers, their transport in the tissues of interest [19] and ways to improve the therapeutic efficacy. Consequently, many studies have reported an increase in the therapeutic efficacy of a drug when coupled with a nano or micro material [20,21] or when particles alone have been introduced to cells to cause antitumor [22] or antibacterial activity [23]. Our model can be used to validate the numerous studies performed relating size dependent cellular uptake and biological effect of nano and micro-material in vitro. For instance, in a study [24] which reported a carrier size-dependent increase in cellular concentration of paclitaxel loaded PLGA particles, decoupling the effect of particle arrival from the reported biological effects could shed more lights on the mechanisms underlying the efficacy of the investigated carriers on the cellular level.

The development of a wide range of drug delivery systems, spanning nano, micro and mesoscopic scales, has resulted in a powerful array of therapeutics. Considerable efforts have been invested in the characterisation of these advanced delivery vectors, however the difference in size between systems has numerous effects, limiting the ability to compare their performance. [25–30] Whilst the

pharmacology of many specific drug delivery vectors is well reported, there is little or no literature on comparative studies, which encompass various scales. Existing reports primarily focus on size[31,32] or shape[33,34] changes within a single drug delivery system. The pronounced surface to volume ratio scaling as size is reduced to the nanoscale affects the physical nature of the particles and their biological effects.[35] As an example, a larger size of the carrier can be linked to a better encapsulation capacity, higher weight of particle, faster sedimentation rate and larger total surface area of individual particles but collectively lower surface area per unit weight. On the other hand, smaller particles are more likely to aggregate and bind more efficiently to surfaces/receptors, when functionalized.[36–38]

The above differences in the physical characteristics of the carriers pose difficulties in comparing the functional biologically/pharmacologically relevant behaviours across the systems, considering similar mass/volume concentration ranges.[39,40] In standard liquid-based cell culture systems, the number of particles associated with cells at any time is a function of the rate of delivery of drug vectors to the cells, the mode of vectors' interaction with the cell surface, and the rates of cellular uptake and loss by degradation or exocytosis. Therefore, the definition of dose for drug vectors in an *in vitro* system is more dynamic, more complicated, and less comparable across particulates than it is for soluble chemicals. Particulates diffuse, agglomerate and settle in cell culture media as a function of their individual properties, such as particle size, shape, surface charge and density; and environmental factors, such as media volume and viscosity. These factors also determine the rate of transport of drug vectors to cells in culture, thus providing a background for biased evaluation of biological responses. For example, Lison *et. al.* demonstrated differences in nominal and effective dose arising from silica particle concentration, media volume and height [39] and Limbach *et. al.* have presented experimental evidence that transport to cells of 25-50 nm and 250-500 nm cerium oxide particles is different, depending in the former case on diffusion and the latter case on gravitational settling.[32] This differential transport was shown to affect cellular uptake rates and

toxicity. In an insightful study Wittmaack showed that a unified description of particle-cell interaction can be obtained despite varying experimental factors, provided that the key determinant of cell response in known. This showed that for nanoparticles a universal response curve can be obtained when presented as a function of areal mass density of particles transported to cells.[41]

In this study, we aim to provide a general framework for the benchmarking of drug vectors of differing materials across size scales, presenting a unified theory for dose-response for an arbitrary drug delivery vehicle. Our approach is based and validated on experimental data obtained using a model system of cationic polyethylene imine (PEI) based macromolecules (mol-PEI), and surface coated nano- and microparticles (NP-PEI and μP-PEI) delivered to Human foreskin fibroblast cells (HFF-1). These delivery vehicles are chosen to span molecular to micro scales and in doing so they account for different modes of delivery to the cell with diffusion dominating molecular transport, diffusion and sedimentation dictating the nanoparticle motion and sedimentation alone being the dominant transport mechanism for the microparticles. As we have previously reported, since PEI has almost immediate biological effects directly related to its contact with the cell membrane, this molecule provides an ideal model for comparing behaviors of various drug vectors.[42,43] We stress that this is not a biology focused study from which we try to understand the cellular response; rather, it is a presentation and validation of a technique for comparing the performance of different scales of drug delivery systems. We show that the delivery kinetics of PEI to the cells is highly correlated with the dynamics of cell death and use the benchmarking analysis to obtain a hypothesis that the magnitude of the biological response to PEI is determined by the total number of PEI molecules delivered to the cells by surface attachment to the various delivery vectors.

2. Methods

Cell culture: Human foreskin fibroblast cells (HFF-1, ATCC® SCRC-1041™) were obtained from American type culture collection (ATCC, Manassas, Virginia, USA). The cells were cultured in 75

cm^2 flasks in a humidified incubator at 37°C with 5% CO_2 in Dulbecco's modified Eagle's medium (DMEM, ATCC) supplemented with 15% fetal bovine serum (FBS, Invitrogen, USA), 4 mM L-glutamine, 1 mM sodium pyruvate and 1% penicillin (50 IU mL^{-1}) /streptomycin (50 μg mL^{-1}).

Delivery vectors: The tested systems included polyethylenimine (PEI, Mw 25,000, density 1.030 g mL^{-1}, Sigma Aldrich, USA), PEI modified nanoparticles (NP-PEI) and PEI modified microparticles (μP-PEI). NP-PEI: PEI modified quantum dots (QD), were synthetized as previously described [42,44]. To obtain μP-PEI, spherical silica beads, (0.9 μm diameter and zeta potential -28.1mV) were obtained from Polysciences Inc. (USA). The beads were sonicated and washed 3-4 times in DI water (followed by centrifugation at 20,000g for 10 min). Further, the supernatant was removed and the microparticles were oxidized with 10% HNO_3 in DI water for 30 min. Following centrifugation and three washes with isopropyl alcohol (IPA), PEI functionalization was performed using 1mL (1.030g) PEI dissolved in 5mL IPA and 250μL DI water. Particles were treated with PEI/IPA/water solution at 35°C with 1300 rpm mixing for 2 h. The particles were washed five times with fresh IPA to remove any residual PEI molecules and re-suspended in the cell media immediately prior to dosing the cells.

Particle characterisation: Both NP-PEI and μP-PEI systems were characterized for zeta potential and hydrodynamic diameter using a Zetasizer Nano ZS (Malvern Corp, Worcestershire, UK). For the analysis, NP-PEI and μP-PEI were suspended in phosphate buffer (PB, pH 7.4) at a concentration of 21 nM the results were recorded in triplicate. PEI-QD diameter was also assessed from scanning electron micrographs.

Time-resolved microscopy, measurement of cell death: Cytotoxicity was quantified using DRAQ7 staining, kindly provided by Biostatus Ltd (UK). Cells were seeded at a concentration of 70,000 cells per well in Greiner Bio One Cellstar® tissue culture 6-well plate for 24 h. The NP-PEI and μP-PEI along with 3μM concentration of DRAQ7 was placed in 2mL of complete medium before being vortexed for 5 sec to ensure thorough mixing. The cells were washed twice in serum-free

medium and incubated with 2 mL of complete medium containing the dose and DRAQ7. High throughput, time-lapse based experiments were performed within 5-10 min of dosing using the In-Cell Analyzer 2000 microscope (*GE* Healthcare, USA). Images were obtained once every hour for 24 h of over 4,000 cells at each time point. Cells were imaged at 20x magnification in two channels: the DRAQ7 channel and the bright-field channel. If NP-PEI were involved in the assay, they were imaged with excitation and emission wavelengths of 350 and 568 nm respectively. At the end of the time-lapse experiment the cells were dosed with a very high dose (10 μM) of NP-PEI in 2 mL media with 0.5 h exposure, which killed 100% of cells in each well. An additional set of images was then collected, from which a measure of the total number of cells in each well was obtained.

Measurement of delivery vector accumulation: The time course of each delivery vector reaching the bottom of a cell culture well was measured using time-lapse microscopy. The wells of a flat base 6 well-Olympus plate (no cells) were dosed with various concentrations of free mol-PEI, NP-PEI and μP-PEI in triplicate. All were suspended in 2mL of DMEM plus 15% FBS. The wells had a diameter of 34.8 mm, which meant that when filled with 2 mL of media the height of the media is 2.1mm. The ImageXpress High-Content Analyzer (Molecular Devices, USA) obtained brightfield images using transmitted white light and also fluorescent images of the NP-PEI using their fluorescent channel (Ex/Em 350/568 nm) on the bottom surface of the well where cells would normally reside. The images were taken once every hour. The media was maintained at a constant temperature of 37°C. ImageJ 1.45 software (National Institutes of Health) was used to manually measure the mean pixel intensity, as pixel intensity can be assumed to be proportional to particle dose at a given time point. The inverse mean pixel intensity of 81 brightfield images of free PEI and μP-PEI was used to quantify the amount of free PEI and μP-PEI, as these are non-fluorescent and produced a dark area within the image.

3. Results

3.1. Characterisation of delivery vectors

Details relating to characterisation of delivery vector size and surface charge are presented in **Figure 1** and summarised in **Table 1**. Coating of the vectors with the 25 kDa PEI produces a cationic surface layer of ~ 15-25 nm thickness with high positive charge (ζ value > +15 mV). The surface charge carried by the PEI is highly disruptive to cells, damaging the lipid membrane and causing rapid death.[43] This direct action of the PEI cargo results in a rapid cellular response and so the temporal dependence of the exposure-response characteristics is determined primarily by the physical processes of vector delivery rather than downstream biological mechanisms.[42] Thus this delivery vector/cargo system is well suited for the development of a generic protocol, focused on the relation of vector size to the delivered cargo dose.

3.2. Exposure-response profiles

We begin our presentation of the cell response profiles with the pharmacological standard of an end-point, exposure-response curve. Data is presented in **Figure 2** on the % cell death after 24 hours of exposure to the three drug vectors, across a range of concentrations. For each delivery system the assay delivers a full description of the concentration dependent cell response. However a common understanding of all three systems through the fundamental mechanisms that determine their cell interactions cannot be obtained directly. It is clear that there is a widely differing potency, dependent upon the vector size. Whilst this could be anticipated, it is difficult to gain any quantitative insight as the ‘delivered dose’ is determined by counteracting effects - a reduced concentration of larger delivery vectors is linked to increased numbers of PEI cargo molecules per vector. Crucially, the measurements cannot report on any of the processes that drive the pharmacodynamics, for this is a single time-point assay.

To overcome these limitations we adopt an alternative approach, based on time-lapse imaging of the cells [42] to obtain time-mortality data.[45] This allows observation of the dynamics of cell response as the delivery vector concentration is increased. Results for all 3 vectors, at varying concentration, taken over a 24 hour exposure period are shown in **Figure 3**. When the cell response is viewed as a temporal process, the influence of the vector delivery becomes immediately apparent. The rapid delivery of the relatively heavy microparticles (μP-PEI) through sedimentation produces a quick response with cell death rapidly increasing and then plateauing within a few hours, regardless of the exposure concentration. In contrast the lighter nanoparticle and molecule systems show slower and more complex dynamics, the form of which is dependent upon the delivery-vector concentration. This is as expected since the delivery in these cases is driven by both sedimentation and diffusion with the relative weighting of these processes dependent upon particle size and density.[46] The response profile for the μP-PEI has a constant form with the % cell death scaling linearly with exposure concentration. This is indicative of a dose-response that is purely delivery dependent with the time to cell death determined by the sedimentation velocity and culture medium height and the maximum % of cells dying controlled by the available particle dose. In all cases there is a saturation in the cell mortality below 100% for lower exposure concentrations and we attribute this to depletion of the delivery vectors from the supply reservoir.[42,46]

Close inspection of the time-mortality curves for NP-PEI and mol-PEI would seem to indicate anomalous results as the time response of the cells is similar whereas the diffusion/sedimentation dynamics of the nanoparticles and molecules should be orders of magnitude different. The response profile is determined by (1) the time dependent arrival of the PEI dose and (2) the susceptibility distribution of the cell population, i.e. the accumulated dose at a particular time point and the heterogeneity in the cells' response to this dose. Thus, to further investigate the results shown in Figure 3 we need to isolate these two factors.

3.3. Delivery vector accumulation dynamics

To decouple the delivery of the PEI vectors from the cell response we assessed their arrival kinetics onto a culture well surface without the presence of cells. Measurement of the relative changes in delivery vector concentration follows from analysis of microscopy images of the well surface. The NP-PEI quantity is assessed by measurement of total nanoparticle fluorescence whereas the μP-PEI and mol-PEI vectors are quantified from analysis of bright-field images. Example images, taken for each delivery vector after 24 hours of accumulation, are shown in **Figure 4**. The fact that the mol-PEI can be directly imaged using optical microscopy indicates that there is substantial agglomeration occurring within the culture medium and that the delivery vector in this case is not molecular in scale at the point of interaction with cells.

Using the diameter of the PEI agglomerates, measured from the microscopy images, we can estimate the mean number of molecules per agglomerate. The average diameter is 930 nm (N = 50) and they have a surface density of 5.2×10^7 cm^{-2}, thus the total number of agglomerates across the 9.5 cm^2 area of the culture well is 49.4×10^7. Assuming that all of the PEI molecules are in an agglomerated form then we estimate a mean number per aggregate of $1.2 \times 10^{16} / 49.4 \times 10^7 = 2.4 \times 10^7$ molecules (total molecule number calculated for 10 μM concentration and 2 ml volume). This total number of molecules, N_{mol} is related to the overall agglomerate size, d_{agg}:

$$N_{mol} = \left(\frac{d_{agg}}{d_{mol}} \right)^3 \quad (1)$$

where d_{mol} is the mean spacing of molecules in the cluster. In this case, d_{mol} = 3.2 nm, which corresponds closely to typical diameters for molecules of this weight (25 kDa),[47] indicating that the PEI has formed tightly packed agglomerates. The dramatically increased 'effective size' of the PEI molecules caused by agglomeration explains the similarity in cellular response dynamics for mol-PEI and NP-PEI seen in Figure 3. The delivery rate of the approximately micron sized PEI

agglomerates is similar to the heavier but smaller quantum dots. An approximate estimate of the sedimentation velocity for the two delivery systems confirms that it is of the same order of magnitude for both (d_{NP} = 15 nm, d_{PEI} = 930 nm, ρ_{NP} = 5.8 g cm^{-3}, ρ_{PEI} = 1.03 g cm^{-3}).

The full time course data is shown in **Figure 5**. In the case of the μP-PEI, where the delivery *in vitro* is sedimentation dominated, the particle velocity is independent of particle concentration and all delivery vectors arrive at the surface within 5 hours. The lighter NP-PEI and mol-PEI systems display an extended characteristic in which the rate of signal increase drops off over time as the vector supply in the solution is reduced. To obtain a reliable metric of the vector accumulation dynamics we fit the data with the equation.[42]

$$s(t) = s_0\left[1 - e^{-t/\tau}\right] \quad (2)$$

Where *S* is the measured signal and S_0 the maximum signal due to all delivery vectors being present at the surface. τ is a characteristic 'accumulation time' that defines the time frame for particle arrival. It describes the dynamics of the system as described by the relative changes in *S*, as in all lifetime-based measures τ is independent of the absolute scaling of *S*. Thus τ can be obtained through secondary measures that are proportional to vector concentration (e.g. fluorescence or brightfield pixel intensity). The accumulation time effectively parameterises the delivery dynamics by quantifying the particle motion resulting from diffusion and sedimentation with a single metric. The equation is derived from a consideration of a closed system with a fixed supply reservoir from which particles are delivered to a surface.[42] The measured data plus modelled fits are shown in Figure 5. Whilst the fits lines do not accurately match the data for all vector concentrations, nonetheless **Equation 2** does provides a realistic description of the curve profiles for all three delivery vector types and scales appropriately across the full range of concentrations.

The formulation and validation of a calibrated vector delivery equation provides a powerful tool with which we can move from exposure metrics to quantification of delivered dose. The measured signal, *S* in Equation 2 can be replaced by the vector number, *N* to which it is linearly correlated:

$$N(t) = CV\left[1 - e^{-t/\tau}\right] \quad (3)$$

Where *C* is the exposure concentration of the vector and *V* the volume of the exposure medium ($CV = N_o$). **Equation 3** can be used to transform time-mortality data into delivered dose-mortality curves using known values of *C* and *V* together with τ values determined from the data fits in Figure 5. The results of this transformation for the three delivery vector systems (data in Figure 3) are shown in **Figure 6**. The cell response is now related to the vector dose accumulated at the cell surface, thus different exposure concentrations (colour-labelled in Figure 6) produce a series of curves that lie on the same profile and extend to a maximum length determined by the concentration (maximum possible dose). This is as expected and a demonstration of Haber's law– the accumulated dose is a product of the concentration of the agent and the duration of exposure.[48] Whilst the form of the delivered dose-mortality curves is similar to the standard exposure-response data taken at t = 24 hours (Figure 2) they differ in one very important aspect: the delivered dose-mortality curves are time independent. In using Equation 3 to remove the kinetics of vector delivery to the cell surface *in vitro* we have obtained response profiles that describe the innate biological susceptibility to the exposure agent. If the correct relationship between delivery vector size and PEI potency can now be obtained then transformation of this delivered dose into a determinant of biological effect (toxicity or mortality) will produce a unified, global response curve that describes the % cell death independent of the form of carrier by which the toxin is delivered.

3.4. Investigating the controlling factor for cellular response

The dose-mortality curves shown in Figure 6 are different for the three delivery vehicle systems. However, in each case it is the same toxic agent, cationic PEI that is causing cell death, thus the differences must stem from the packing of the agent on each delivery vehicle. The data, therefore, describe a secondary factor related to the presentation of the PEI molecules to the cells rather than the primary cell-toxin interaction. However, the delivered dose-mortality curves do provide a means by which various hypotheses on the form of this primary interaction can be investigated. If we can correctly identify the mechanism of toxicity and find the mathematical relationship that links it to the delivered drug vehicle dose then we can transform the individual response curves for different delivery systems into a single, global curve of drug response, independent of the means by which the drug reaches the cell.

The first step in this investigation addresses the fact that the PEI agglomerates when in molecular form. The concentration of the delivered mol-PEI used in Figure 6 must, therefore, be corrected to report the *effective* agglomerated vector concentration rather than that predicted under the assumption of a monodisperse molecular solution. This is simply done by dividing the delivered dose value by our estimate of the mean number of PEI molecules per agglomerate ($N = 2.4x10^7$). The results of this transformation are shown in **Figure 7A**. The role of the delivery vector size now becomes very apparent as the mol-PEI and μP-mol systems, which have near equal diameters, show nearly identical dose-mortality profiles. Even with agglomeration the concentration of mol-PEI remains higher than that of the μP-mol (maximum concentration of 16,000 *f*M *cf.* 300 *f*M) and so the data extends over the full % range for cell death in this case.

The data in Figure 7A shows that an equivalent cell response is produced by PEI molecules when they are attached to the surface of a micron scale particle and when they aggregate into a molecular cluster of the same dimensions. This observation leads to the hypothesis that it is the availability of PEI at the surface of the delivery vector that determines the level of toxicity. To test this hypothesis

we calculated the mean number of surface PEI molecules per vector using the measured vector diameters (microparticle = 950 nm, molecular agglomerate = 930 nm, nanoparticle = 15 nm) and an assumed PEI spacing of 3.2 nm. The calculated values were then converted into a molar concentration by multiplying by the effective vector dose concentration (independent variable in Figure 7A). The result of this dose metric transform is shown in **Figure 7B**. A unified result is indeed obtained with all delivery vector types and exposure concentrations producing a dose-mortality curve that sits on the same global profile. This confirms the hypothesis that it is the total number of PEI molecules presented to the cell on a delivery vector surface, which determines the level of cellular toxicity. The curve in Figure 7B is graphical evidence of the potential of this benchmarking approach for comparison of drug delivery vehicles, regardless of their material composition or size, and the extraction of the true therapeutic/toxic interaction of the drug/toxin with cells.

4. Discussion

Optimal drug delivery necessitates selective use of particular delivery vehicles, chosen from a wide range of candidate designs and materials dependent upon the nature of the drug and its specified target, and so techniques for benchmarking pharmacological performance across systems are essential. This poses a significant challenge in separating the multiple processes and mechanisms that determine a dose-response profile and which are dependent upon the delivery vector characteristics and the toxicity of its cargo. The time resolved analysis that we present provides a measurement based technique for separating these processes.

By implementing a simple, phenomenological, vector reservoir model we are able to accurately describe the arrival of delivery vectors at the cell surface, allowing us to transform a time-dependence into a dose accumulation. This crucial step separates the processes of drug delivery and drug activity *in vitro* and avoids the complicated dynamics of particle motion in solution[40] by directly determining the resultant dose without need to consider the delivery process. Using this transformation of data from an exposure-response form to a delivered dose-response profile, comparisons can be made of the effectiveness of different drug delivery vectors, according to their presentation of the drug to cells rather than their efficiency of delivery. This allows an understanding of the influence of drug packaging by a carrier vector upon the response of a biological system. Indeed, when fully implemented the benchmarking procedure can provide a single, global drug response metric that identifies the determinant of drug potency and quantifies its influence according to the chosen carrier vector.

The implementation of delivery vector benchmarking presented here has allowed us to compare the free delivery of a cationic molecule to carrier-based delivery using nano and microscale particles. The technique enables us to infer the presence of agglomeration of the free molecules from the time-resolved cellular response data and to identify the total number of molecules attached to the delivery vector surface as the primary factor determining cell death. The protocol can be implemented across a wide range of delivery vectors, regardless of morphology, scale and composition and is reliant only on the ability to perform time-resolved cellular response studies. Wider adoption of this approach would allow multiscale, cross-material comparisons of drug delivery vectors and optimisation of therapeutic effect based on analysis of the primary mechanism of drug action rather than secondary factors such as packing density on the delivery vehicle or the efficiency and speed of delivery.

References

1. Langer R. Drug delivery and targeting. *Nature*. 392(6679 Suppl), 5–10 (1998).

2. Byers JP, Sarver JG. Pharmacokinetic Modeling. *Pharmacology*. 201-277 (2009).

3. Allen TM, Cullis PR. Drug delivery systems: entering the mainstream. *Science*. 303(5665), 1818–1822 (2004).

4. Faraji AH, Wipf P. Nanoparticles in cellular drug delivery. Bioorganic Med. Chem. 17(8), 2950–2962 (2009).

5. Tasciotti E, Liu X, Bhavane R, *et al.* Mesoporous silicon particles as a multistage delivery system for imaging and therapeutic applications. *Nat. Nanotechnol.* 3(3), 151–157 (2008).

6. Davis ME, Chen ZG, Shin DM. Nanoparticle therapeutics: an emerging treatment modality for cancer. *Nat. Rev. Drug Discov.* 7(9), 771–782 (2008).

7. Ferrari M. Cancer nanotechnology: opportunities and challenges. *Nat. Rev. Cancer*. 5(3), 161–171 (2005).

8. McNeil SE. Nanoparticle therapeutics: A personal perspective. *Wiley Interdiscip. Rev. Nanomedicine Nanobiotechnology*. 1(3), 264–271 (2009).

9. Otto DP, Otto A, Villiers MM De, de Villiers MM. Differences in physicochemical properties to consider in the design, evaluation and choice between microparticles and nanoparticles for drug delivery. *Expert Opin. Drug Deliv.* 1–15 (2014).

10. Doak SH, Griffiths SM, Manshian B, *et al.* Confounding experimental considerations in nanogenotoxicology. *Mutagenesis*. 24(4), 285–293 (2009).

11. Soenen SJ, Rivera-Gil P, Montenegro JM, Parak WJ, De Smedt SC, Braeckmans K. Cellular toxicity of inorganic nanoparticles: Common aspects and guidelines for improved nanotoxicity evaluation. *Nano Today*. 6, 446–465 (2011).

12. Oberdörster G. Safety assessment for nanotechnology and nanomedicine: Concepts of nanotoxicology. *J. Intern. Med.* 267(1), 89–105 (2010).

13. Kroll A, Dierker C, Rommel C, *et al.* Cytotoxicity screening of 23 engineered nanomaterials using a test matrix of ten cell lines and three different assays. *Part. Fibre Toxicol.* 8(1), 9 (2011).

14. Sohaebuddin SK, Thevenot PT, Baker D, Eaton JW, Tang L. Nanomaterial cytotoxicity is composition, size, and cell type dependent. *Part. Fibre Toxicol.* 7, 22 (2010).

15. Carlson C, Hussain SM, Schrand AM, *et al.* Unique Cellular Interaction of Silver Nanoparticles: Size-Dependent Generation of Reactive Oxygen Species. *J. Phys. Chem. B* 112(43), 13608–13619 (2008).

16. Kim JA, Åberg C, Salvati A, Dawson K a. Role of cell cycle on the cellular uptake and dilution of nanoparticles in a cell population. *Nat. Nanotechnol.* 7(1), 62–8 (2012).

17. Marco M Di, Shamsuddin S, Razak KA, *et al.* Overview of the main methods used to combine proteins with nanosystems: Absorption, bioconjugation, and encapsulation. *Int. J. Nanomedicine*. 5(1), 37–49 (2010).

18. Steinbacher JL, Landry CC. Adsorption and release of siRNA from porous silica. *Langmuir*. 30, 4396–405 (2014).

19. He C, Yin L, Tang C, Yin C. Size-dependent absorption mechanism of polymeric nanoparticles for oral delivery of protein drugs. *Biomaterials*. 33(33), 8569–78 (2012).

20. Hwu JR, Lin YS, Josephrajan T, *et al.* Targeted Paclitaxel by conjugation to iron oxide and gold nanoparticles. *J. Am. Chem. Soc.* 131(1), 66–68 (2009).

21. Xu Z, Gu W, Huang J, *et al.* In vitro and in vivo evaluation of actively targetable nanoparticles for paclitaxel delivery. *Int. J. Pharm.* 288, 361–368 (2005).

22. Gurunathan S, Han JW, Eppakayala V, Jeyaraj M, Kim J-H. Cytotoxicity of biologically synthesized silver nanoparticles in MDA-MB-231 human breast cancer cells. *Biomed Res. Int.* 2013, 535796 (2013).

23. Ivask A, Kurvet I, Kasemets K, *et al.* Size-dependent toxicity of silver nanoparticles to bacteria, yeast, algae, crustaceans and mammalian cells in vitro. *PLoS One.* 9(7), e102108 (2014).

24. Chakravarthi SS, De S, Miller DW, Robinson DH. Comparison of anti-tumor efficacy of paclitaxel delivered in nano- and microparticles. *Int. J. Pharm.* 383, 37–44 (2010).

25. Barbé C, Bartlett J, Kong L, *et al.* Silica particles: A novel drug-delivery system. *Adv. Mater.* 16(21), 1959–1966 (2004).

26. Kataoka K, Harada A, Nagasaki Y. Block copolymer micelles for drug delivery: design, characterization and biological significance. *Adv. Drug Deliv. Rev.* 47(1), 113–131 (2001).

27. Agnihotri SA, Mallikarjuna NN, Aminabhavi TM. Recent advances on chitosan-based micro- and nanoparticles in drug delivery. J. Control. Release. 100(1), 5–28 (2004).

28. Bianco A, Kostarelos K, Prato M. Applications of carbon nanotubes in drug delivery. Curr. Opin. Chem. Biol. 9(6), 674–679 (2005).

29. Rosenholm JM, Peuhu E, Bate-Eya LT, Eriksson JE, Sahlgren C, Lindén M. Cancer-cell-specific induction of apoptosis using mesoporous silica nanoparticles as drug-delivery vectors. *Small*. 6(11), 1234–1241 (2010).

30. Dobson J. Magnetic micro- and nano-particle-based targeting for drug and gene delivery. *Nanomedicine (Lond).* 1(1), 31–37 (2006).

31. Moghimi SM, Hunter a C, Andresen TL. Factors controlling nanoparticle pharmacokinetics: an integrated analysis and perspective. *Annu. Rev. Pharmacol. Toxicol.* [Internet]. 52, 481–503 (2012). Available from: http://www.ncbi.nlm.nih.gov/pubmed/22035254.

32. Limbach LK, Li Y, Grass RN, *et al.* Oxide nanoparticle uptake in human lung fibroblasts: effects of particle size, agglomeration, and diffusion at low concentrations. *Environ. Sci. Technol.* 39(23), 9370–9376 (2005).

33. Florez L, Herrmann C, Cramer JM, *et al.* How shape influences uptake: Interactions of anisotropic polymer nanoparticles and human mesenchymal stem cells. *Small*. 8(14), 2222–2230 (2012).

34. Champion JA, Katare YK, Mitragotri S. Particle shape: A new design parameter for micro- and nanoscale drug delivery carriers. J. Control. Release. 121(1-2), 3–9 (2007).

35. Whitesides GM. The “right” size in nanobiotechnology. *Nat. Biotechnol.* 21(10), 1161–1165 (2003).

36. Basu S, Ghosh SK, Kundu S, *et al.* Biomolecule induced nanoparticle aggregation: Effect of particle size on interparticle coupling. *J. Colloid Interface Sci.* 313(2), 724–734 (2007).

37. Walkey CD, Olsen JB, Guo H, Emili A, Chan WCW. Nanoparticle size and surface chemistry determine serum protein adsorption and macrophage uptake. *J. Am. Chem. Soc.* 134(4), 2139–2147 (2012).

38. Chithrani BD, Ghazani A a., Chan WCW. Determining the size and shape dependence of gold nanoparticle uptake into mammalian cells. *Nano Lett.* 6(4), 662–668 (2006).

39. Lison D, Thomassen LCJ, Rabolli V, *et al.* Nominal and effective dosimetry of silica nanoparticles in cytotoxicity assays. *Toxicol. Sci.* 104(1), 155–162 (2008).

40. Teeguarden JG, Hinderliter PM, Orr G, Thrall BD, Pounds JG. Particokinetics in vitro: Dosimetry considerations for in vitro nanoparticle toxicity assessments. *Toxicol. Sci.* 95(2), 300–312 (2007).

41. Wittmaack K. Novel dose metric for apparent cytotoxicity effects generated by in vitro cell exposure to silica nanoparticles. *Chem. Res. Toxicol.* 24, 150–158 (2011).

42. Ware MJ, Godin B, Singh N, *et al.* Analysis of the influence of cell heterogeneity on nanoparticle dose response. *ACS Nano*. 8(7), 6693–700 (2014).

43. Mecke A, Majoros IJ, Patri AK, Baker JR, Holl MMB, Orr BG. Lipid bilayer disruption by polycationic polymers: the roles of size and chemical functional group. *Langmuir*. 21(23), 10348–54 (2005).

44. Romoser A, Ritter D, Majitha R, Meissner KE, McShane M, Sayes CM. Mitigation of quantum dot cytotoxicity by microencapsulation. *PLoS One*. 6(7), 1–7 (2011).

45. BLISS CI, Stevens WL. THE CALCULATION OF THE TIME-MORTALITY CURVE. *Ann. Appl. Biol.*. 24(4), 815–852 (2008).

46. Hinderliter PM, Minard KR, Orr G, *et al.* ISDD: A computational model of particle sedimentation, diffusion and target cell dosimetry for in vitro toxicity studies. *Part. Fibre Toxicol.* 7(1), 36 (2010).

47. Erickson HP. Size and shape of protein molecules at the nanometer level determined by sedimentation, gel filtration, and electron microscopy. *Biol. Proced. Online*. 11(1), 32–51 (2009).

48. Gaylor DW. The use of Haber's Law in standard setting and risk assessment. *Toxicology*. 149(1), 17–19 (2000).

Figure Captions:

Table 1: Size and zeta potential parameters of the delivery vectors and PEI cargo.

Figure 1: (A) Electron micrograph of NP-PEI; (B) NP-PEI size histogram based on electron micrograph; (C & D) Electron micrograph of bare μP and μP-PEI respectively.

Figure 2: Exposure-response curves after 24 hours of exposure for micro, nano and molecular delivery vectors.

Figure 3: Time-mortality curves for (A) μP-PEI; (B) NP-PEI and (C) mol-PEI treated HFF-1 cells. Arrows indicate direction of increasing exposure concentration; μP-PEI: control (red), uncoated – 31 fM (magenta), coated – 8 fM (blue), 15 fM (green), 31 fM (yellow), 76 fM (black), 153 fM (red), 306 fM (blue); NP-PEI: control (green), 1 nM (red), 2 nM (black), 3 nM (magenta), 4.5 nM (red), 5 nM (blue), 6 nM (black), 18 nM (blue), 45 nM (magenta); mol-PEI: control (red), 0.4 μM (green),4 μM (black),10 μM (blue), 20 μM (magenta), 40 μM (green), 200 μM (blue), 400 μM (red). The error bars show the standard error in the mean (n=3).

Figure 4: Bright field (mol-PEI and μP-PEI) and fluorescence (NP-PEI) images of delivery vector accumulation on the culture well surface. Each image is of a 387x387 μm area.

Figure 5: Time resolved arrival of delivery vectors onto the culture well surface for (A) μP-PEI, (B) NP-PEI and (C) mol-PEI. The solid lines show a modelled fit using the indicated characteristic delivery time, τ (see Equation 2).

Figure 6: Dose-mortality curves calculated by transformation of data in Figure 3, using equation 2. Exposure concentrations used are; μP-PEI: 15,31,76,153 fM; NP-PEI: 3,4.5,6,18 nM; mol-PEI: 10,20,40,200 μM.

Figure 7: Biological response (% of cell death) as a function of: (A) effective vector dose concentration and (B) the solution concentration of the PEI molecules that are present at the surface of the delivery vectors. Legend: μP-PEI (blue symbols), NP-PEI (red symbols) and mol-PEI (green symbols), original data shown in Figure 6.

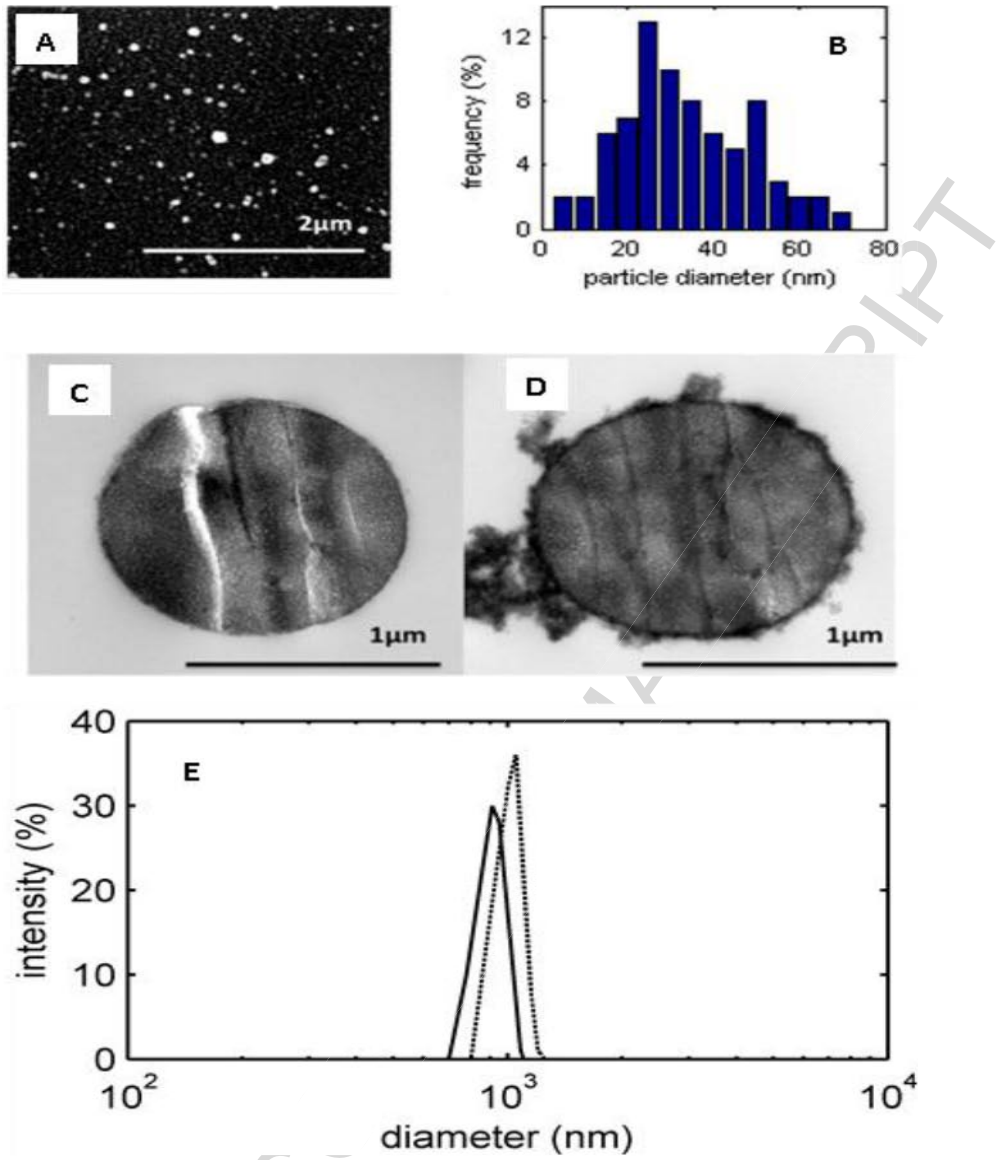
A
2µm
B
frequency (%)
12
8
4
0
0
20
40
60
80
particle diameter (nm)
C
1µm
D
1µm
E
intensity (%)
40
30
20
10
0
10^2
10^3
10^4
diameter (nm)

Figure 1

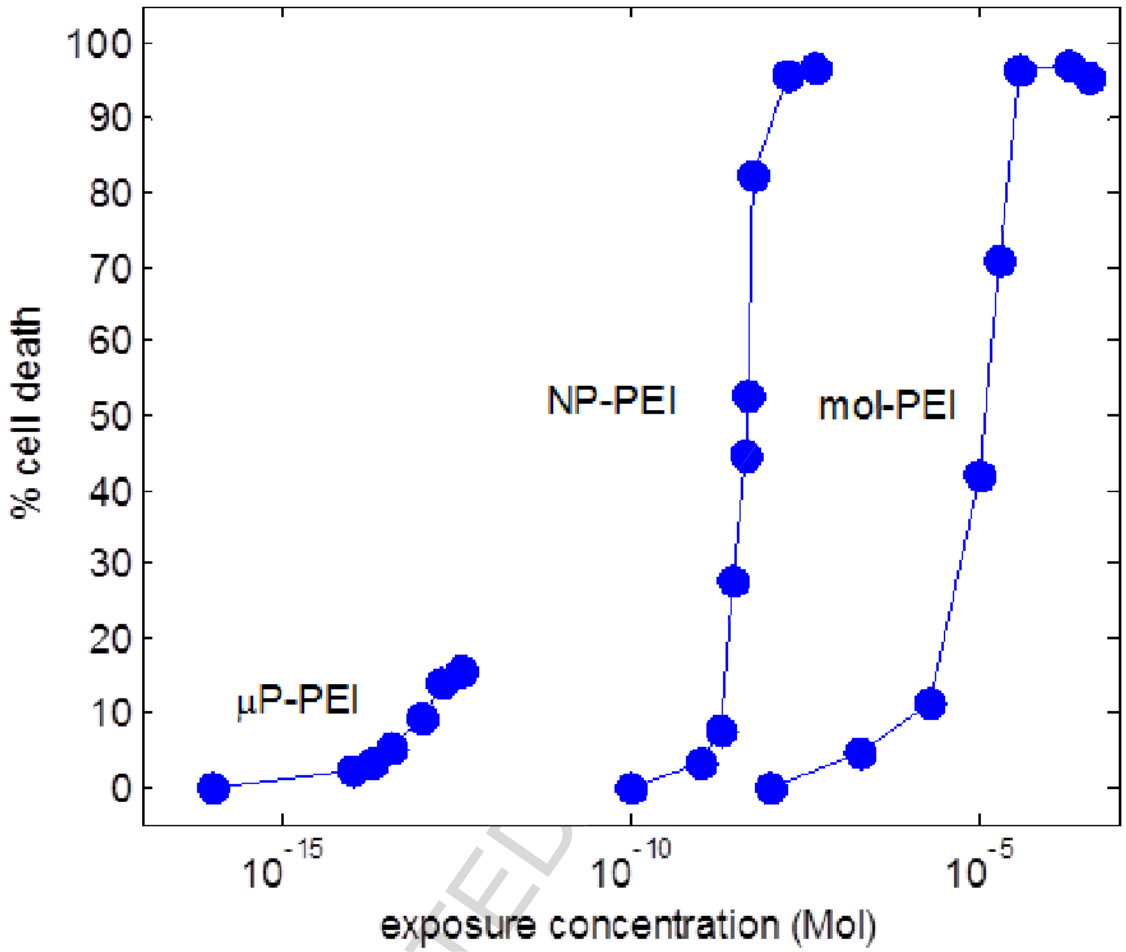

Figure 2

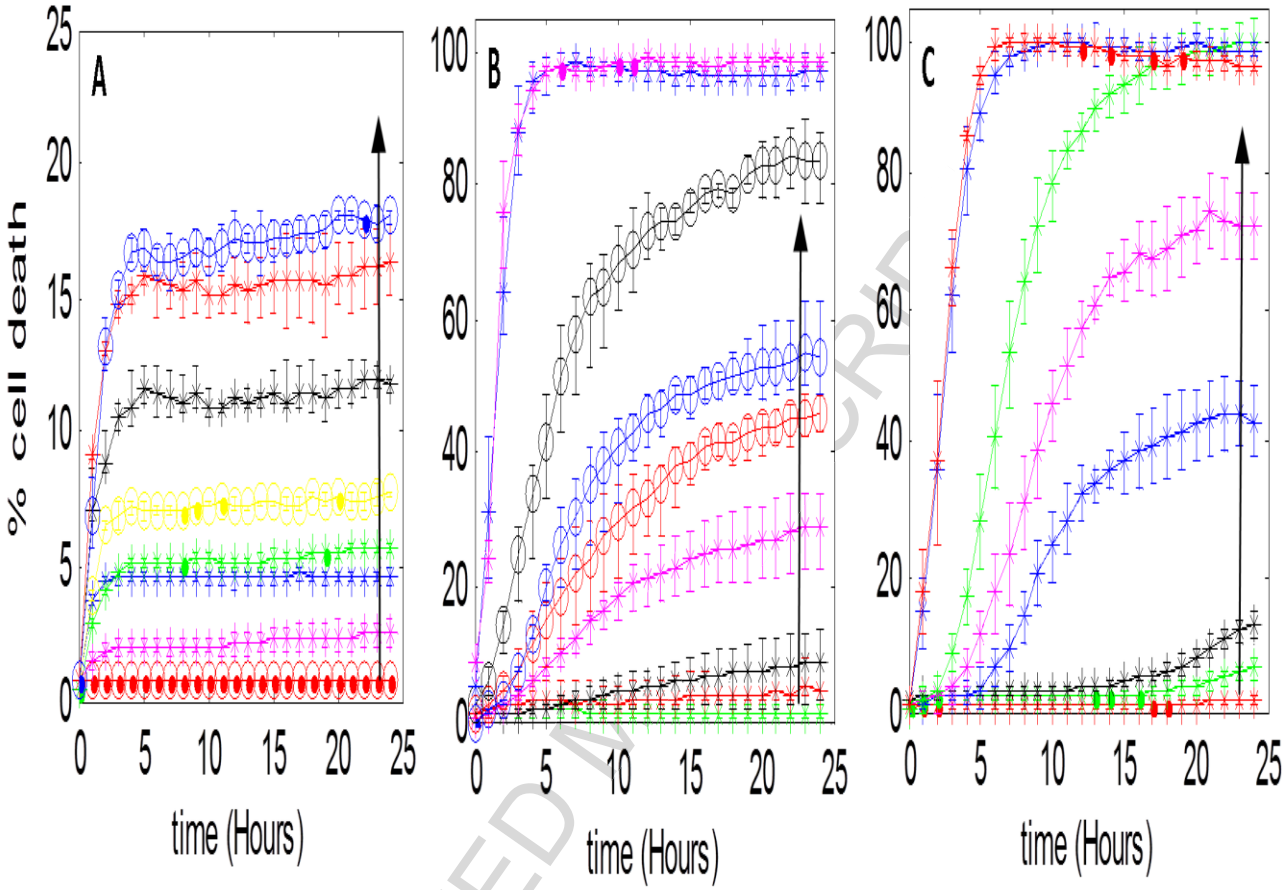

Figure 3

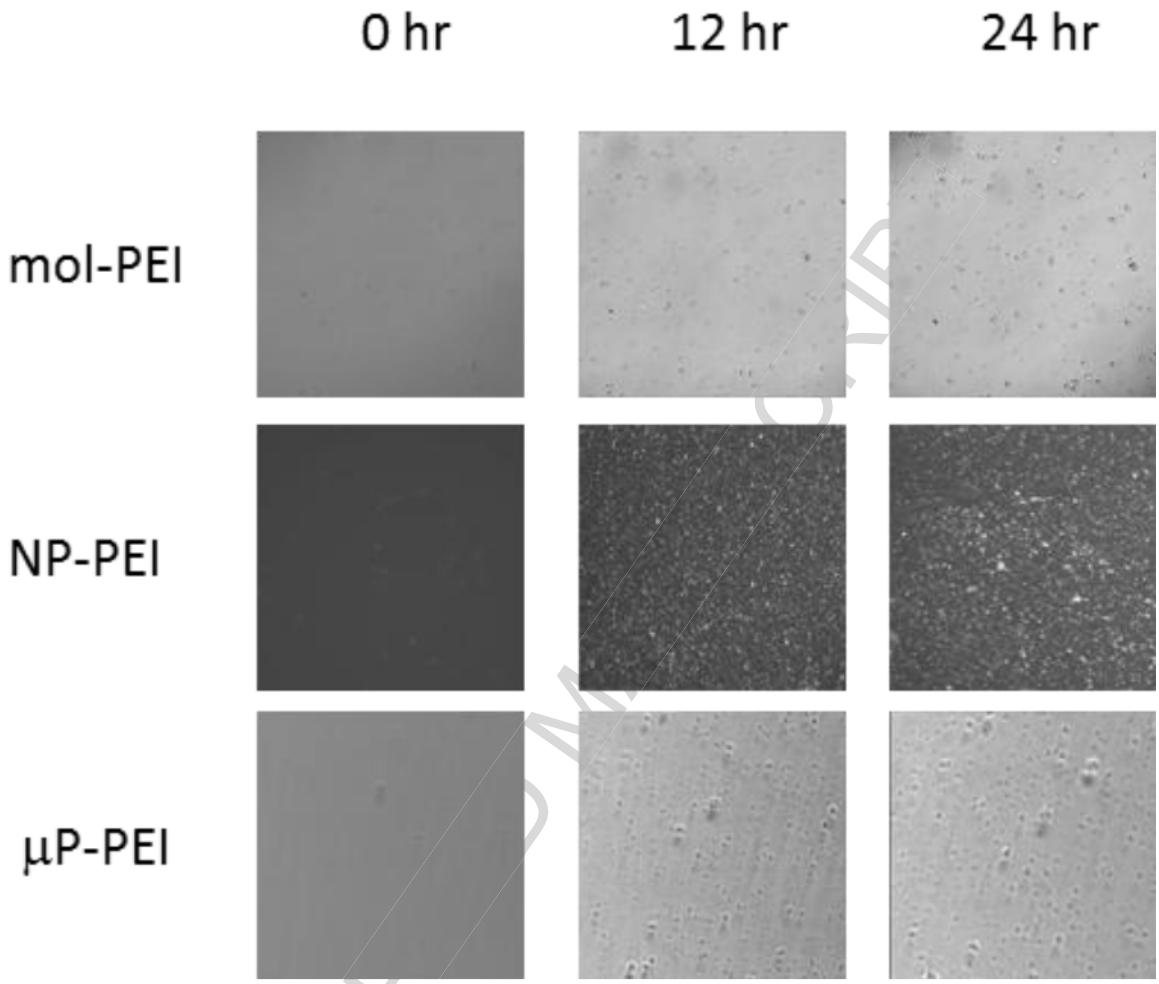

Figure 4

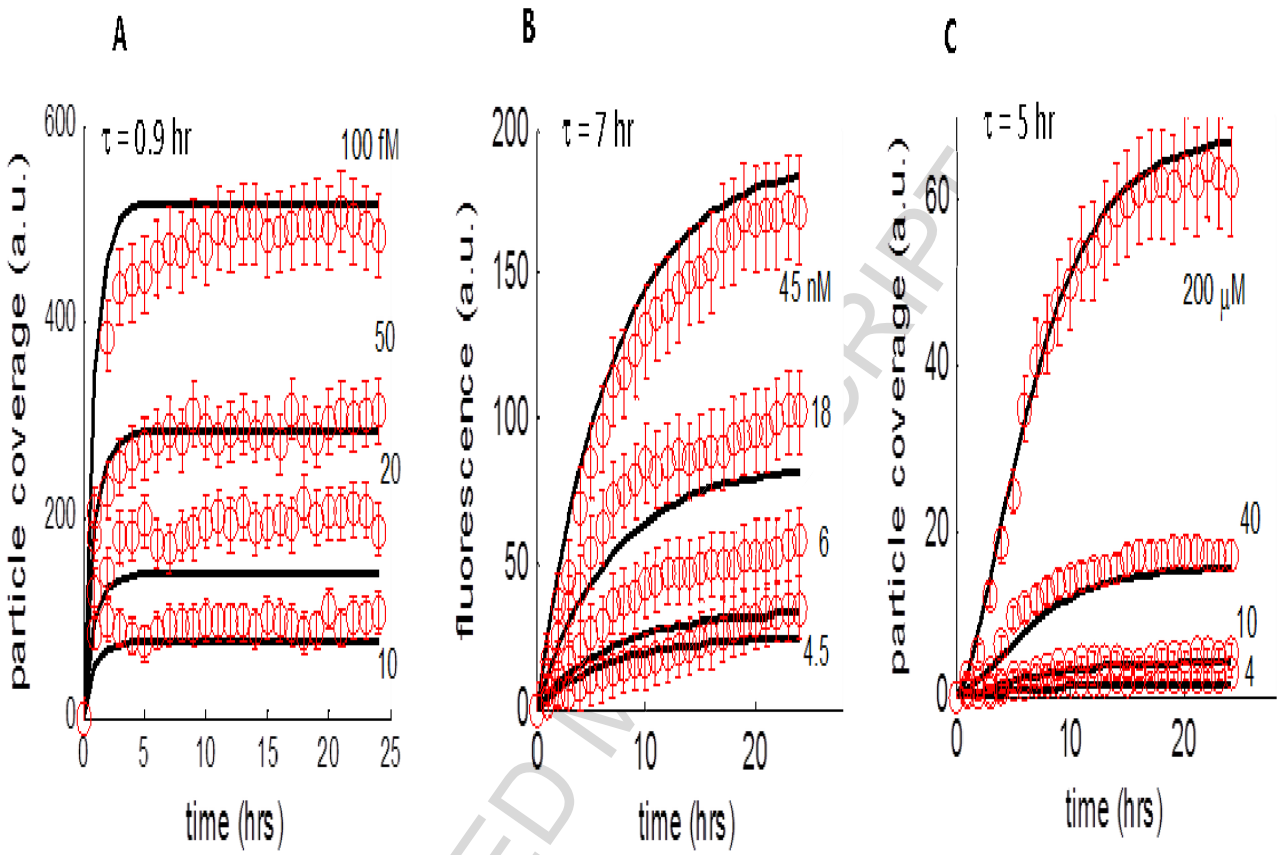

Figure 5

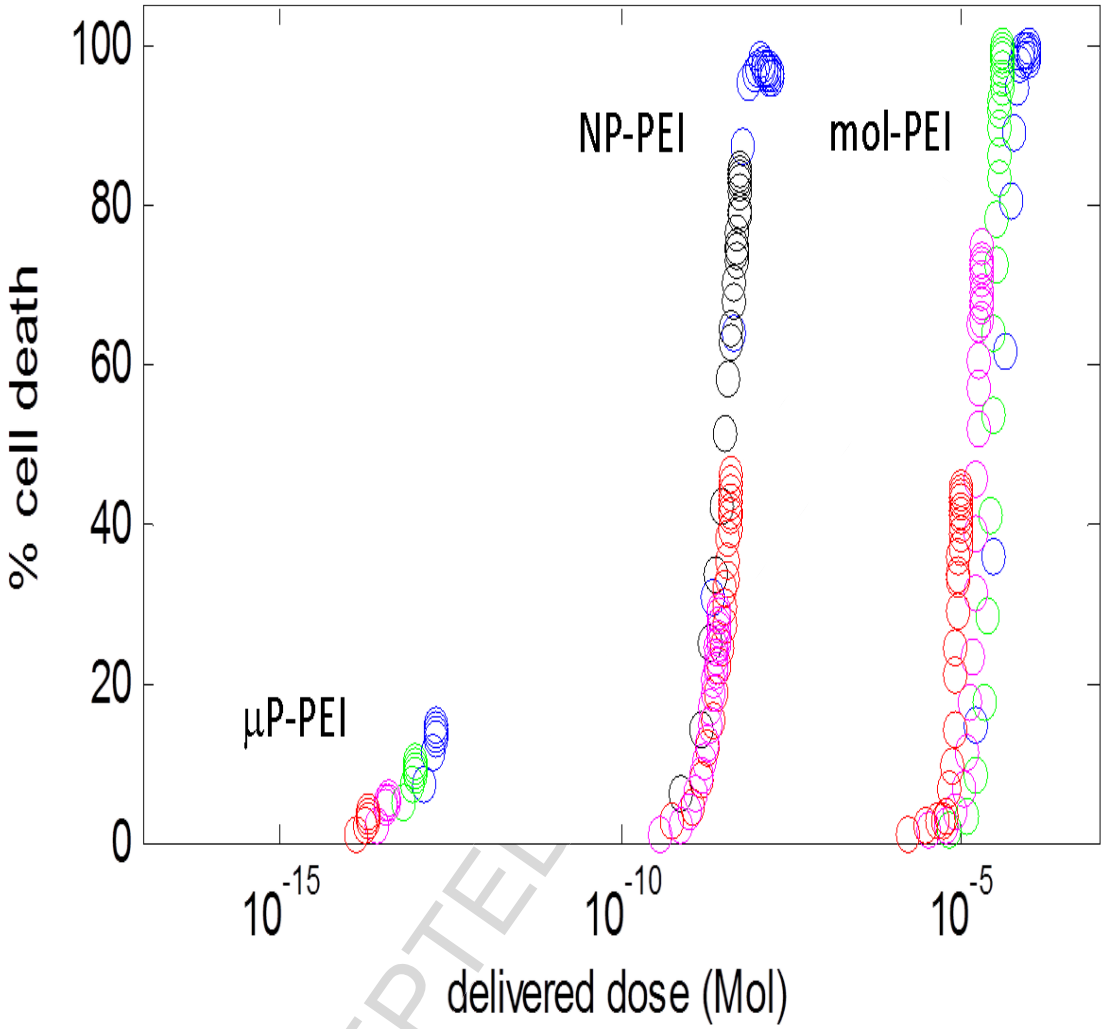

Figure 6

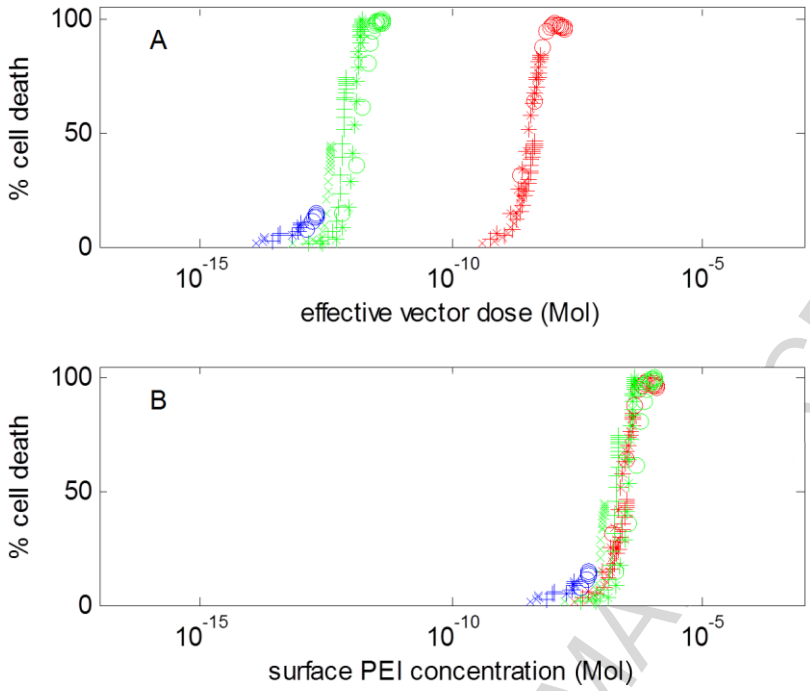

Figure 7

Graphical Abstract

Many of the key advances in Nanomedicine relate to the concept of delivery of a drug via a secondary carrier – a delivery vector. Here we present an experimental approach that allows quantitative comparison of delivery vectors across scales. This allows detailed analysis and discrimination of the relative roles of the carrier and the drug in determining cell response.

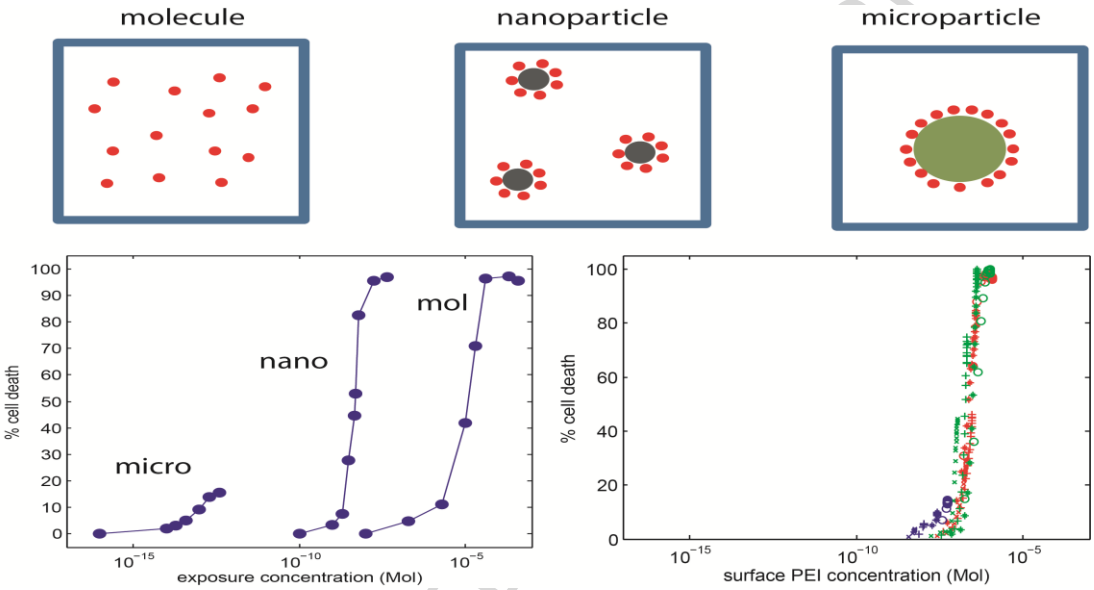

Table 1: Size and zeta potential parameters of the delivery vectors and PEI cargo.

Delivery vector	Size (nm) Bare particle (PEI coated form)	Zeta-potential (mV)
µP-PEI, microparticle	950 (1100)	+ 15.2 +/- 5.2
NP-PEI, nanoparticle	15[a] (34)	+ 18.6 +/- 5.7
PEI, molecule	25 kDa weight	

[a] *value reported in* [44]